
Article:
Alsharkawi, A. and Rossiter, J.A. orcid.org/0000-0002-1336-0633 (2017) Towards an Improved Gain Scheduling Predictive Control Strategy for a Solar Thermal Power Plant. IET Control Theory and Applications. ISSN 1751-8644

https://doi.org/10.1049/iet-cta.2016.1319

Towards an Improved Gain Scheduling Predictive Control Strategy for a Solar Thermal Power Plant

Adham Alsharkawi[1,*] and Anthony Rossiter[2]

[1]Department of Automatic Control and Systems Engineering, University of Sheffield, Sheffield, S1 3JD, UK
[2]Department of Automatic Control and Systems Engineering, University of Sheffield, Sheffield, S1 3JD, UK
[*]aalsharkawi1@sheffield.ac.uk

Abstract: This paper improves a recently proposed gain scheduling predictive control strategy on the ACUREX distributed solar collector field at the Plataforma Solar de Almería. Measured disturbances are an integral part of the plant and while simple classical, series and parallel, feedforward approaches have been proposed and used extensively in the literature, the proposed approach incorporates a feedforward systematically into the predictive control strategy by including the effects of the measured disturbances of the ACUREX plant into the predictions of future outputs. Models of the measured disturbances are estimated around a family of operating points from input-output data and using a subspace identification method while taking into account the frequency response of the plant. Input-output data are obtained from a validated nonlinear simulation model of the plant rather than the plant itself. The nonlinear simulation model is validated against measured data obtained from the ACUREX plant and the effectiveness of the proposed control approach is evaluated in the same nonlinear simulation environment. The paper also considers the impact of incorporating the future behaviour of a measured disturbance along a given prediction horizon, a theme which has received little attention in the literature.

1. Introduction

ACUREX is a parabolic trough technology-based solar thermal power plant. One of the biggest challenges of such a plant is to maintain the field outlet temperature at a desired level despite changes, mainly in solar radiation and the field inlet temperature [1].

1.1. The Use of Feedforward with ACUREX Distributed Solar Collector Field

Solar radiation and the field inlet temperature act as measured disturbances to the plant and hence it is not surprising that many feedforward approaches have been proposed over the years to compensate for their effects.

One of the early approaches can be traced back to the early nineties of the last century when two simple alternatives, series and parallel feedforward compensation, were proposed [2]. Both alternatives are derived from a nonlinear lumped parameter model of the ACUREX plant at steady-state conditions. Experimental data were used to determine some unknown parameters. A similar approach is proposed in [3] to compensate for changes in solar radiation. A static version of a

nonlinear plant model is used and two unknown parameters had to be found experimentally while the plant was in equilibrium using standard optimization techniques. Changes in the field inlet temperature are compensated for dynamically by simple transfer functions. Series and parallel feedforward compensation were assessed and it was found that in contrast to the series feedforward compensation, the parallel feedforward compensation resulted in poor set point tracking. In [4], measurements of solar radiation and field inlet temperature were used in an adaptive predictive control strategy. Measurements of solar radiation pass through a filter in an attempt to mitigate the fast changes in solar radiation. The parallel feedforward compensation in [2] is used in [5] for the design of a dynamic compensation of the field inlet temperature and a simple proportional compensation of solar radiation. The dynamic compensator includes a low pass filter and a delay term and the proportional compensator is based upon the deviation of the measured solar radiation from an estimated value.

By the beginning of a new century, a static version of a model that describes the internal energy of the plant is used to compensate for changes in the field inlet temperature and solar radiation [6]. A few years later, a feedforward based on steady-state energy balance was proposed in [7]; the feedforward compensates for changes in the field inlet temperature and solar radiation and includes a field inlet-outlet temperature time delay. The time delay depends on the flow rate of the HTF and the length of the receiver tube. It is claimed that taking explicit account of the field inlet-outlet temperature time delay improves the feedforward capabilities in terms of compensating for changes in the field inlet temperature. In [8] and after performing some simplifications and Taylor series expansions to a nonlinear distributed parameter model of the plant, transfer functions relating the dynamics of the field inlet temperature and solar radiation to the field outlet temperature are obtained. The transfer functions are used for the design of a classical parallel feedforward compensation. However, the use of the obtained transfer functions was not straightforward since they have exponential expressions that had to be simplified using a first order Padé approximation and, due to the noncausal nature of the obtained feedforward controllers, a causal version of the resulting controllers had to be implemented. More recently, changes in solar radiation are considered in [9] as a load disturbance and incorporated into a first order plus dead-time model of the plant. The effect of solar radiation is modelled as a gain times the variation of the current incident solar radiation with respect to an initial value of the incident solar radiation.

In [10], it was argued that the ACUREX distributed collector field possesses resonance characteristics, namely resonant modes that lie well within the desired control bandwidth and the resonance phenomena arise due to the relatively slow flow rate of the HTF and the length of the receiver tube involved. It was also found that the phenomena have a significant impact on the control performance and hence modelling the resonant modes sufficiently accurately is crucial to ensure high control performance with adequate robustness. More importantly however, it was noticed (using experimental data) that the dynamics relating the field outlet temperature to changes in solar radiation are very similar to the dynamics relating the field outlet temperature to changes in the volumetric flow rate of the HTF and yet, non of the feedforward approaches listed earlier has explicitly appreciated this fact and utilised its potential for control implications.

1.2. Paper Contribution

This paper aims to confirm the experimental findings in [10] and then builds on this to show that also fast and abrupt changes in the field inlet temperature can in fact excite the resonance dynamics of the plant. The paper also aims to demonstrate that incorporating sufficient dynamic models of the field inlet temperature and solar radiation, that take explicit account of the resonance phenom-

ena of the plant, can significantly improve the control performance during the transient phase, set point tracking and disturbance rejection. Finally, focus is given to an area that has received little or no attention in the literature by considering the impact of incorporating the *expected* future behaviour of the measured disturbances along a given prediction horizon. In summary, bringing all these aspects together, the main contribution of this paper, is to improve a gain scheduling (GS) predictive control strategy proposed in [11] by incorporating a systematic feedforward design to compensate for the measured disturbances of the ACUREX plant.

This paper is organised as follows: Mathematical models of the plant are described in Section 2. Section 3 is devoted to system identification and models of the measured disturbances. Section 4 outlines the proposed model-based predictive control (MPC) design. Section 5 shows some simulation results and discusses the main findings. Finally, concluding remarks are presented in Section 6.

2. Mathematical Models

This section gives a brief description of a nonlinear distributed parameter model used for simulation and analysis purposes followed by a simpler nonlinear lumped parameter model which is used solely for control design purposes.

2.1. Nonlinear Distributed Parameter Model

The dynamic behaviour of the plant can be described by the following set of energy balance partial differential equations (PDEs):

$$\begin{array}{l} \rho_m C_m A_m \frac{\partial T_m}{\partial t} = n_o G I - D_o \pi H_l (T_m - T_a) - D_i \pi H_t (T_m - T_f) \\ \rho_f C_f A_f \frac{\partial T_f}{\partial t} + \rho_f C_f q \frac{\partial T_f}{\partial x} = D_i \pi H_t (T_m - T_f) \end{array} \tag{1}$$

where the subindex m refers to the metal of the receiver tube and f to the HTF [1]. Table 1 gives a description of all the variables and parameters and lists their SI units.

2.1.1. Construction of a nonlinear simulation model: A nonlinear simulation model of the plant has been constructed in [12] by dividing the receiver tube into N segments each of length Δx and hence the nonlinear distributed parameter model in (1) has been approximated by the following set of ordinary differential equations (ODEs):

$$\begin{array}{l} \rho_m C_m A_m \frac{dT_{m,n}}{dt} = n_o G I - D_o \pi H_l (T_{m,n} - T_a) - D_i \pi H_t (T_{m,n} - T_{f,n}) \\ \rho_f C_f A_f \frac{dT_{f,n}}{dt} + \rho_f C_f q \frac{T_{f,n} - T_{f,n-1}}{\Delta x} = D_i \pi H_t (T_{m,n} - T_{f,n}) \end{array} , \quad n = 1, ..., N \tag{2}$$

with the boundary condition $T_{f,0} = T_{f,inlet}$ (field inlet temperature) and H_l,H_t,ρ_f and C_f being time−varying. It has been shown [12] that dividing the receiver tube into 7 segments ($N = 7$) is a reasonable trade-off between the prediction accuracy and computational burden while still adequate enough to capture the resonant modes of the plant.

2.1.2. Validation of the nonlinear simulation model: The nonlinear simulation model proposed in (2) is validated in this paper against measured data obtained from the ACUREX plant. The measured data was collected on 15 July 2003 and after a series of step changes in the volumetric flow rate of the HTF. During the data collection, the number of active loops were 9 and mirror optical efficiency (n_o) was 56%.

Table 1 Variables and parameters.

Symbol	Description	SI unit
ρ	Density	kg/m^3
C	Specific heat capacity	$J/kg°\mathrm{C}$
A	Cross-sectional area	m^2
T	Temperature	$°\mathrm{C}$
t	Time	s
I	Solar radiation	W/m^2
n_o	Mirror optical efficiency	$-$
G	Mirror optical aperture	m
D_o	Outer diameter of the receiver tube	m
H_l	Global coefficient of thermal losses	$W/m°\mathrm{C}$
T_a	Ambient temperature	$°\mathrm{C}$
D_i	Inner diameter of the receiver tube	m
H_t	Coefficient of metal-fluid heat transfer	$W/m^2°\mathrm{C}$
q	HTF volumetric flow rate	m^3/s
x	Space	m

Fig. 1 shows the measured inputs (measured disturbances and manipulated variable) to the ACUREX plant and Fig. 2 shows the measured output against model output. One can notice that the measured disturbances have experienced significant changes during the early stage of the flow rate changes and yet, the model output, as shown in Fig. 2, is still able to capture the main dynamics with slight deviation from the measured output. Once the measured disturbances have almost settled, the model output can be clearly seen converging smoothly to the measured output. In summary, the nonlinear simulation model described by the system in (2) is accurate enough for simulation and analysis purposes.

Remark 1. It is worth noting that the field outlet temperature at the ACUREX plant is measured far away from the solar collector field at the end of a return tube which implies slight changes to the dynamics at the solar collector field and more importantly a variable dead-time. Hence, as the nonlinear simulation model represents the outlet temperature at the solar collector field and for a fair comparison, the model output is validated against the outlet temperature of collector loop 5 which is located at the middle of the solar collector field and has the maximum temperature of the ten collector loops. More information about the variable dead-time problem can be found in [13] along with other supplementary dynamics of the plant.

2.2. Nonlinear Lumped Parameter Model

The dynamic behaviour of the ACUREX plant can also be described (approximately) by a simple nonlinear lumped parameter model. Variation in the internal energy of the fluid can be described by:

$$C\frac{dT_f}{dt} = n_o SI - QP_{cp}(T_f - T_{f,inlet}) - H_l(T_{mean} - T_a) \tag{3}$$

where S is the collectors' solar field effective surface, Q is the HTF volumetric flow rate, P_{cp} is a factor that takes into account some geometrical and thermal properties and T_{mean} is the mean of T_f and $T_{f,inlet}$ [1].

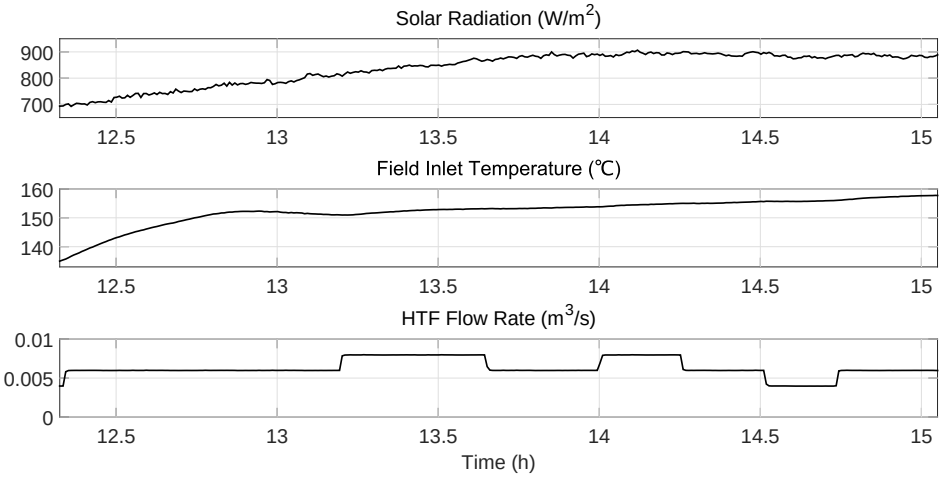

Fig. 1: Measured inputs to the ACUREX plant.

Remark 2. For a given operating point, a local model of the measured disturbances of the ACUREX plant can be derived from first principles using the nonlinear lumped parameter model in (3). Under the assumption that the volumetric flow rate of the HTF (q) is no longer a variable (assuming steady-state condition) and with proper adjustment of the factor P_{cp} to compensate for the heat losses ($H_l(T_{mean} - T_a)$), the variation of the internal energy of the fluid can be given as:

$$\frac{dT_f}{dt} = C_1 T_f + C_2 T_{f,inlet} + C_3 I \tag{4}$$

where $C_1 = \frac{-P_{cp}q}{C}$, $C_2 = \frac{P_{cp}q}{C}$ and $C_3 = \frac{n_o S}{C}$.

The dynamic model in (4) is a typical first-order ordinary differential equation (ODE) with multiple inputs ($T_{f,inlet}$ and I) and single output (T_f) which can be easily represented in a discrete-time state space form.

3. System Identification and Models of the Measured Disturbances

It has been discussed in Section 1 that the dynamics of the measured disturbances of the ACUREX plant have been underestimated in the literature. More specifically, the link between the resonant modes of the plant and the dynamics of the measured disturbances has not been fully appreciated. Hence, in this section, an approach towards an effective modelling of the measured disturbances of the ACUREX plant is proposed. The proposed approach makes use of system identification and takes into account the frequency response of the plant.

3.1. System Identification

Due to the nonlinearity of the ACUREX plant, local LTI state space models relating the volumetric flow rate of the HTF (q) to the field outlet temperature (T_f) were estimated in [11] directly from input-output data around the operating points $q = 0.004$, 0.006, 0.008 and 0.010 m^3/s. Predictions of these models are improved here by estimating models of the field inlet temperature ($T_{f,inlet}$) and solar radiation (I) around the same operating points.

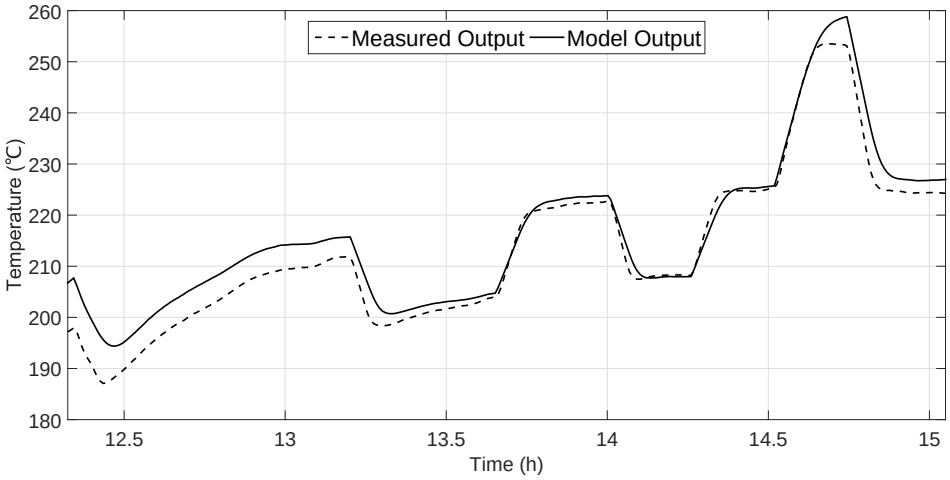

Fig. 2: Measured output against model output.

The nonlinear simulation model of the plant described by the system in (2) was excited with a set of full-length PRBS signals with a clock period equal to the process sampling time 39 s (the process time constant is around 6 min). The identification process was carried out separately for the field inlet temperature and solar radiation and a data set of 1100 samples was used for each of the nominal operating points.

3.2. Models of the Measured Disturbances

Compact local LTI state space models of the field inlet temperature and solar radiation were identified around the nominal operating points using the subspace identification method N4SID discussed in [14]. The general form of a discrete-time LTI state space model is given as:

$$\begin{aligned} x_{k+1} &= Ax_k + Bu_k + \xi_k \\ y_k &= Cx_k + Du_k + \eta_k \end{aligned} \tag{5}$$

where $x_k \in \mathbb{R}^{n\times 1}$, $u_k \in \mathbb{R}^{m\times 1}$, $y_k \in \mathbb{R}^{l\times 1}$, $\xi_k \in \mathbb{R}^{n\times 1}$ and $\eta_k \in \mathbb{R}^{l\times 1}$ are the state vector, input vector, output vector, process noise and measurement noise respectively at discrete time instant k. A, B, C and D are the coefficient matrices of appropriate dimensions.

Models of the field inlet temperature and solar radiation were estimated under the assumptions that there is no direct feedthrough from the input to the output ($D = 0$) and the system is deterministic ($\xi_k = \eta_k = 0$). Model order was estimated by inspecting the singular values of a covariance matrix constructed from the observed data.

Model order and best fit criterion are shown in Table 2 for the field inlet temperature and in Table 3 for solar radiation. Models 1, 2, 3, and 4 refer to the nominal operating points $q = 0.004$, 0.006, 0.008 and 0.010 m^3/s respectively.

The best fit criterion reflects the ability of the estimated models to reproduce the main dynamics of the plant at a given operating point and time horizon. The ability to capture the resonance dynamics of the plant in the model is validated by inspecting the frequency response of the estimated models. Fig. 3 and Fig. 4 show the bode plots of the estimated models and one can clearly identify the resonant modes of the plant and observe the dependence of their frequencies on the flow rate of the HTF.

Table 2 Model order and best fit criterion ($T_{f,inlet}$)

Model	Model order	Best fit criterion (%)
1	5^{th}	96.56
2	7^{th}	97.48
3	7^{th}	97.91
4	7^{th}	98.16

Table 3 Model order and best fit criterion (I)

Model	Model order	Best fit criterion (%)
1	4^{th}	97.97
2	4^{th}	98.51
3	5^{th}	98.77
4	5^{th}	98.91

Indeed, fast and abrupt changes in the field inlet temperature can excite the resonance dynamics of the plant, especially at low flow rates, and as expected the dependence of the dynamics of the field outlet temperature on solar radiation is very similar to the dependence of the dynamics of the field outlet temperature on volumetric flow rate of the HTF.

4. Control Design

A predictive control strategy, namely dual mode MPC is proposed in [15] for the deterministic state space case and used in [11] within a gain scheduling framework. In this section, the dual mode MPC proposed in [15] is extended to include the effects of the measured disturbances of the ACUREX plant.

4.1. Dual Mode MPC

As mentioned earlier, the main contribution of this paper is to improve the GS predictive control strategy proposed in [11], where local dual mode MPC controllers were designed around the nominal operating points q = 0.004, 0.006, 0.008 and 0.010 m^3/s. The design steps of each of the local controllers can be summarised as follows [1]:

- For a deterministic version of the system in (5) and assuming no direct feedthrough from the input to the output, the deviations $\bar{x}_k, \bar{y}_k, \bar{u}_k$ from some an estimated steady-state values x_{ss}, u_{ss} and y_{ss} can be expressed as:

$$\begin{aligned} \bar{x}_{k+1} &= A\bar{x}_k + B\bar{u}_k \\ \bar{y}_k &= C\bar{x}_k \end{aligned} \tag{6}$$

- Hence, a standard dual mode cost function (online performance measure) J is given as [15]:

$$J = \sum_{i=0}^{n_c-1} \left[\bar{x}_{k+1+i}^T \delta\bar{x}_{k+1+i} + \bar{u}_{k+i}^T \lambda \bar{u}_{k+i}\right] + \bar{x}_{k+n_c}^T P \bar{x}_{k+n_c} \tag{7}$$

[1] Detailed treatment of the dual mode MPC and proper definitions of the various variables and parameters can be found in [15].

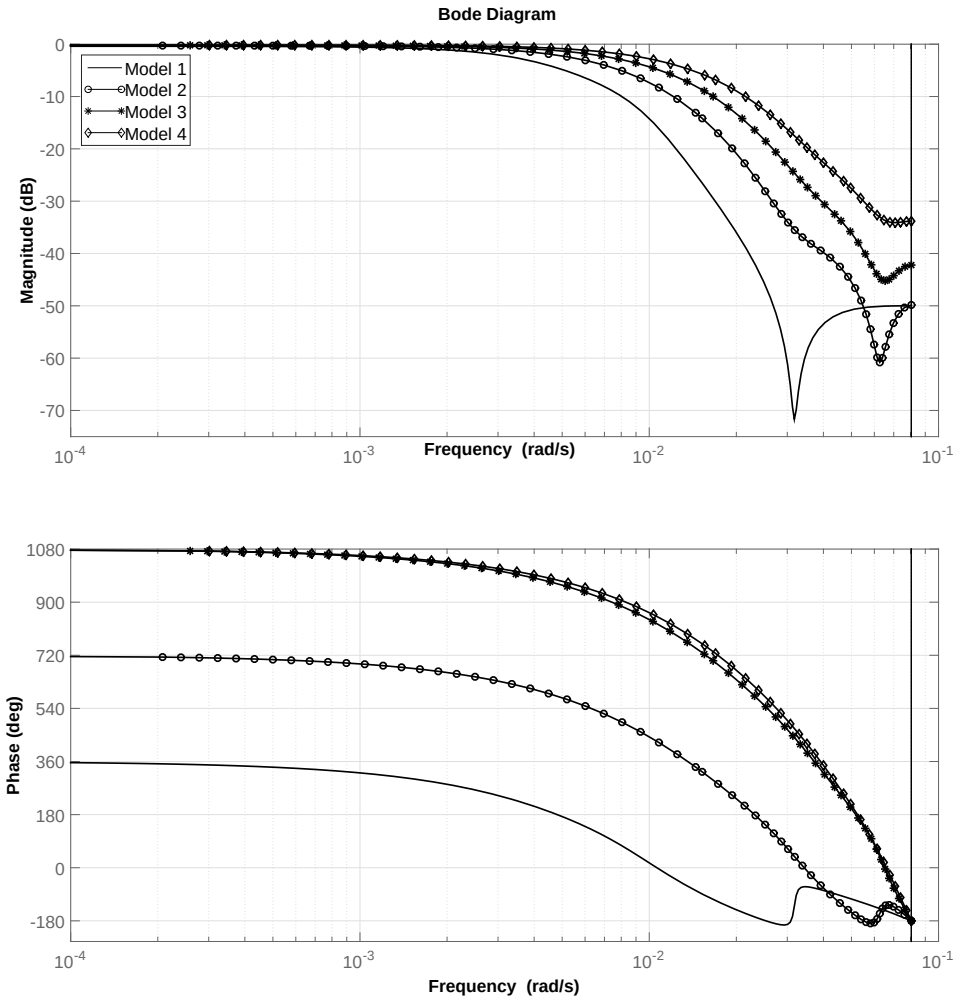

Fig. 3: Bode plots: Estimated models of the field inlet temperature.

where n_c is the number of free d.o.f., δ and λ are weighting matrices of appropriate dimensions and P is the terminal weight obtained from an appropriate Lyapunov equation.

- Optimisation of the cost function in (7) subject to system predictions meeting constraints can be simplified (details omitted as standard in the literature) to take the form of a quadratic programming problem and solved online as:

$$\min_{\underset{\rightarrow}{\bar{u}}} \quad \underset{\rightarrow k-1}{\bar{u}}^T S \underset{\rightarrow k-1}{\bar{u}} + \underset{\rightarrow k-1}{\bar{u}}^T L \bar{x}_k \quad \text{s.t.} \quad \beta \underset{\rightarrow}{\bar{u}} \leq \gamma \tag{8}$$

where $\underset{\rightarrow k-1}{\bar{u}} = [\bar{u}_k^T \quad \bar{u}_{k+1}^T \quad \ldots \quad \bar{u}_{k+n_c-1}^T]^T$, S and L depend upon the matrices A, B, δ, λ and P, β is time-invariant and γ depends upon the system past input-output information.

The design steps can be summarised by the following algorithm.

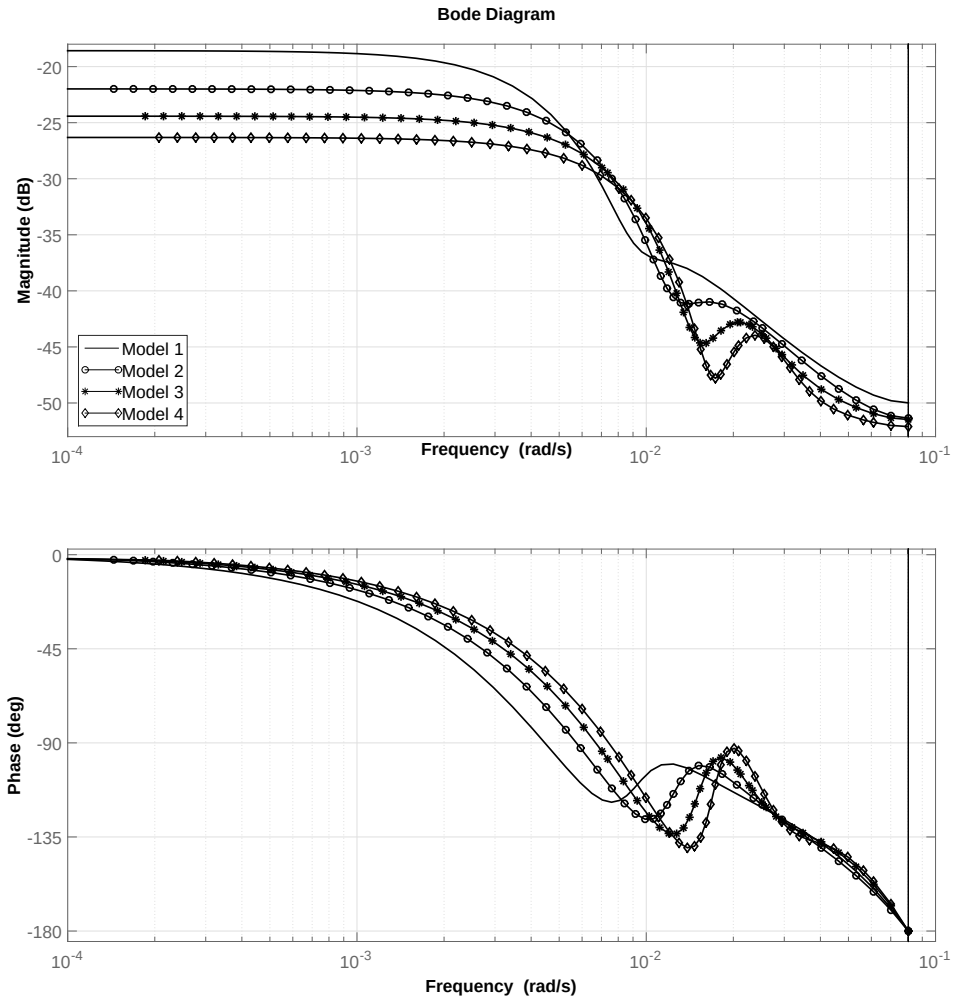

Fig. 4: Bode plots: Estimated models of solar radiation.

Local dual mode MPC (LMPC)

1: Given an operating point and the local process model in (6), define the parameters in (8).
2: At each sampling instant, perform the optimization in (8).
3: Solve for the first element of $\underset{\rightarrow}{\bar{u}}$ and implement on process.

Note that the LMPC can be easily modified to cover a wide range of operation through gain scheduling [11].

GS dual mode MPC (GSMPC)

1: For each of the nominal operating points and given the local process model in (6), define the parameters in (8)
2: For a selected local controller and at each sampling instant, perform the optimization in (8).
3: Solve for the first element of $\underset{\rightarrow}{\bar{u}}$ and implement on process.

The LMPC and GSMPC are improved next by including the dynamics of the measured disturbances.

4.2. Feedforward Dual Mode MPC

In order to include the dynamics of the measured disturbances, slight but essential modifications, to the local process model in (6) need to be made.

Remark 3. The local process model in (6) can be augmented to include the disturbance dynamics as follows:

$$\begin{aligned}
\underbrace{\begin{bmatrix} \bar{x}_{k+1} \\ \bar{x}^{d_1}_{k+1} \\ \bar{x}^{d_2}_{k+1} \end{bmatrix}}_{\bar{z}_{k+1}} &= \underbrace{\begin{bmatrix} A & 0 & 0 \\ 0 & A^{d_1} & 0 \\ 0 & 0 & A^{d_2} \end{bmatrix}}_{\bar{A}} \underbrace{\begin{bmatrix} \bar{x}_k \\ \bar{x}^{d_1}_k \\ \bar{x}^{d_2}_k \end{bmatrix}}_{\bar{z}_k} + \underbrace{\begin{bmatrix} B & 0 & 0 \\ 0 & B^{d_1} & 0 \\ 0 & 0 & B^{d_2} \end{bmatrix}}_{\bar{B}} \begin{bmatrix} \bar{u}_k \\ \bar{d}_{1k} \\ \bar{d}_{2k} \end{bmatrix} \\
\bar{\psi}_k &= \underbrace{\begin{bmatrix} C & C^{d_1} & C^{d_2} \end{bmatrix}}_{\bar{C}} \underbrace{\begin{bmatrix} \bar{x}_k \\ \bar{x}^{d_1}_k \\ \bar{x}^{d_2}_k \end{bmatrix}}_{\bar{z}_k}
\end{aligned} \tag{9}$$

where the subindices d_1 and d_2 indicate that the system has two measured disturbances. $\bar{d}_1$ and $\bar{d}_2$ at sample time k are the deviations of the measured disturbances d_1 and d_2 from some an estimated steady-state values d_{1ss} and d_{2ss} respectively.

Appropriate modifications to the dual mode cost function in (7) and consequently the optimisation in (8) depend upon the assumptions made about the future of the measured disturbances.

Theorem 1. If the future behaviour of the measured disturbances along a given prediction horizon is considered and given the augmented local process model in (9), then the optimisation in (8) is extended as follows:

$$\min_{\underset{\rightarrow}{\bar{u}}} \quad \underset{\rightarrow k-1}{\bar{u}^T} S \underset{\rightarrow k-1}{\bar{u}} + \underset{\rightarrow k-1}{\bar{u}^T} L \bar{z}_k + \underset{\rightarrow k-1}{\bar{u}^T} M \underset{\rightarrow k-1}{\bar{d}_1} + \underset{\rightarrow k-1}{\bar{u}^T} N \underset{\rightarrow k-1}{\bar{d}_2} \quad \text{s.t.} \quad \beta \underset{\rightarrow}{\bar{u}} \leq \gamma \tag{10}$$

where S and L in this case depend upon the matrices $\bar{A}$, B, δ, λ and P, M depends upon the matrices $\bar{A}$, B, B^{d1}, δ and P, and similarly N depends upon the matrices $\bar{A}$, B, B^{d2}, δ and P.

Proof. Under the assumption that the first n_c control moves are free and that the remaining moves are given by a fixed feedback law, let the predictions be:

$$\begin{aligned}
z_{k+i} &= \bar{A} z_{k+i-1} + B u_{k+i-1} + B^{d_1} d_{1k+i-1} + B^{d_2} d_{2k+i-1}; \quad u_{k+i-1} \text{ are d.o.f.}, \quad i = 1, ..., n_c \\
z_{k+i} &= [\bar{A} - BK] z_{k+i-1} + B^{d_1} d_{1k+i-1} + B^{d_2} d_{2k+i-1}; \quad u_{k+i-1} = -K z_{k+i-1}, \quad i > n_c
\end{aligned} \tag{11}$$

Now given some steady-state estimates z_{ss}, u_{ss}, d_{1ss} and d_{2ss} and under the assumption that $d_{1k+i-1} = d_{1ss}$ and $d_{2k+i-1} = d_{2ss}$, $\forall i > n_c$, then the deviation of z_{k+i}, $\forall i$ can be expressed as:

$$\begin{aligned}
\bar{z}_{k+i} &= \bar{A} \bar{z}_{k+i-1} + B \bar{u}_{k+i-1} + B^{d_1} \bar{d}_{1k+i-1} + B^{d_2} \bar{d}_{2k+i-1} \\
\bar{z}_{k+i} &= [\bar{A} - BK] \bar{z}_{k+i-1}
\end{aligned} \tag{12}$$

and hence, it is convenient to separate the cost:

$$J = \sum_{i=0}^{\infty} \bar{z}^T_{k+1+i} \delta \bar{z}_{k+1+i} + \bar{u}^T_{k+i} \lambda \bar{u}_{k+i} \tag{13}$$

into two parts as follows:

$$J = J_1 + J_2; \qquad \begin{aligned} J_1 &= \sum_{i=0}^{n_c-1} \bar{z}_{k+1+i}^T \delta \bar{z}_{k+1+i} + \bar{u}_{k+i}^T \lambda \bar{u}_{k+i} \\ J_2 &= \sum_{i=0}^{\infty} \bar{z}_{k+n_c+1+i}^T \delta \bar{z}_{k+n_c+1+i} + \bar{u}_{k+n_c+i}^T \lambda \bar{u}_{k+n_c+i} \end{aligned} \tag{14}$$

Note that one can form the whole vector of future predictions up to a horizon n_c as follows:

$$\begin{aligned} \underbrace{\begin{bmatrix} \bar{z}_{k+1} \\ \bar{z}_{k+2} \\ \bar{z}_{k+3} \\ \vdots \\ \bar{z}_{k+n_c} \end{bmatrix}}_{\underset{\rightarrow k}{\bar{z}}} &= \underbrace{\begin{bmatrix} \bar{A} \\ \bar{A}^2 \\ \bar{A}^3 \\ \vdots \\ \bar{A}^{n_c} \end{bmatrix}}_{W_x} \bar{z}_k + \underbrace{\begin{bmatrix} B & 0 & 0 & \cdots \\ \bar{A}B & B & 0 & \cdots \\ \bar{A}^2B & \bar{A}B & B & \cdots \\ \vdots & \vdots & \vdots & \vdots \\ \bar{A}^{n_c-1}B & \bar{A}^{n_c-2}B & \bar{A}^{n_c-3}B & \cdots \end{bmatrix}}_{H_x} \underbrace{\begin{bmatrix} \bar{u}_k \\ \bar{u}_{k+1} \\ \bar{u}_{k+2} \\ \vdots \\ \bar{u}_{k+n_c-1} \end{bmatrix}}_{\underset{\rightarrow k-1}{\bar{u}}} \\ &+ \underbrace{\begin{bmatrix} B^{d_1} & 0 & 0 & \cdots \\ \bar{A}B^{d_1} & B^{d_1} & 0 & \cdots \\ \bar{A}^2B^{d_1} & \bar{A}B^{d_1} & B^{d_1} & \cdots \\ \vdots & \vdots & \vdots & \vdots \\ \bar{A}^{n_c-1}B^{d_1} & \bar{A}^{n_c-2}B^{d_1} & \bar{A}^{n_c-3}B^{d_1} & \cdots \end{bmatrix}}_{F_x} \underbrace{\begin{bmatrix} \bar{d}_{1k} \\ \bar{d}_{1k+1} \\ \bar{d}_{1k+2} \\ \vdots \\ \bar{d}_{1k+n_c-1} \end{bmatrix}}_{\underset{\rightarrow k-1}{\bar{d}_1}} \\ &+ \underbrace{\begin{bmatrix} B^{d_2} & 0 & 0 & \cdots \\ \bar{A}B^{d_2} & B^{d_2} & 0 & \cdots \\ \bar{A}^2B^{d_2} & \bar{A}B^{d_2} & B^{d_2} & \cdots \\ \vdots & \vdots & \vdots & \vdots \\ \bar{A}^{n_c-1}B^{d_2} & \bar{A}^{n_c-2}B^{d_2} & \bar{A}^{n_c-3}B^{d_2} & \cdots \end{bmatrix}}_{G_x} \underbrace{\begin{bmatrix} \bar{d}_{2k} \\ \bar{d}_{2k+1} \\ \bar{d}_{2k+2} \\ \vdots \\ \bar{d}_{2k+n_c-1} \end{bmatrix}}_{\underset{\rightarrow k-1}{\bar{d}_2}} \end{aligned} \tag{15}$$

Hence, substituting (15) into J_1 in (14) gives:

$$\begin{aligned} J_1 = &[W_x \bar{z}_k + H_x \underset{\rightarrow k-1}{\bar{u}} + F_x \underset{\rightarrow k-1}{\bar{d}_1} + G_x \underset{\rightarrow k-1}{\bar{d}_2}]^T \mathrm{diag}(\delta) [W_x \bar{z}_k + H_x \underset{\rightarrow k-1}{\bar{u}} + F_x \underset{\rightarrow k-1}{\bar{d}_1} + G_x \underset{\rightarrow k-1}{\bar{d}_2}] \\ &+ \underset{\rightarrow k-1}{\bar{u}}^T \mathrm{diag}(\lambda) \underset{\rightarrow k-1}{\bar{u}} \end{aligned} \tag{16}$$

and according to [15]:

$$J_2 = [W_{nc} \bar{z}_k + H_{nc} \underset{\rightarrow k-1}{\bar{u}} + F_{nc} \underset{\rightarrow k-1}{\bar{d}_1} + G_{nc} \underset{\rightarrow k-1}{\bar{d}_2}]^T P [W_{nc} \bar{z}_k + H_{nc} \underset{\rightarrow k-1}{\bar{u}} + F_{nc} \underset{\rightarrow k-1}{\bar{d}_1} + G_{nc} \underset{\rightarrow k-1}{\bar{d}_2}] \tag{17}$$

where W_{nc}, H_{nc}, F_{nc} and G_{nc} are the nc^{th} block rows of W_x, H_x, F_x and G_x respectively.

Finally one can combine J_1 and J_2 from (16) and (17) to give:

$$\begin{aligned} J = &[W_x \bar{z}_k + H_x \underset{\rightarrow k-1}{\bar{u}} + F_x \underset{\rightarrow k-1}{\bar{d}_1} + G_x \underset{\rightarrow k-1}{\bar{d}_2}]^T \mathrm{diag}(\delta) [W_x \bar{z}_k + H_x \underset{\rightarrow k-1}{\bar{u}} + F_x \underset{\rightarrow k-1}{\bar{d}_1} + G_x \underset{\rightarrow k-1}{\bar{d}_2}] \\ &+ \underset{\rightarrow k-1}{\bar{u}}^T \mathrm{diag}(\lambda) \underset{\rightarrow k-1}{\bar{u}} + [W_{nc} \bar{z}_k + H_{nc} \underset{\rightarrow k-1}{\bar{u}} + F_{nc} \underset{\rightarrow k-1}{\bar{d}_1} + G_{nc} \underset{\rightarrow k-1}{\bar{d}_2}]^T P [W_{nc} \bar{z}_k + H_{nc} \underset{\rightarrow k-1}{\bar{u}} + F_{nc} \\ &\underset{\rightarrow k-1}{\bar{d}_1} + G_{nc} \underset{\rightarrow k-1}{\bar{d}_2}] \end{aligned} \tag{18}$$

which can be simplified to:

$$J = \underset{\rightarrow k-1}{\bar{u}}^T \underbrace{[H_x^T \mathrm{diag}(\delta) H_x + \mathrm{diag}(\lambda) + H_{nc}^T P H_{nc}]}_{S} \underset{\rightarrow k-1}{\bar{u}} + \underset{\rightarrow k-1}{\bar{u}}^T \underbrace{2[H_x^T \mathrm{diag}(\delta) W_x + H_{nc}^T P W_{nc}]}_{L} \bar{z}_k$$
$$+ \underset{\rightarrow k-1}{\bar{u}}^T \underbrace{2[H_x^T \mathrm{diag}(\delta) F_x + H_{nc}^T P F_{nc}]}_{M} \underset{\rightarrow k-1}{\bar{d}_1} + \underset{\rightarrow k-1}{\bar{u}}^T \underbrace{2[H_x^T \mathrm{diag}(\delta) G_x + H_{nc}^T P G_{nc}]}_{N} \underset{\rightarrow k-1}{\bar{d}_2} + \alpha \tag{19}$$

where α does not depend on $\underset{\rightarrow k-1}{\bar{u}}$. □

Remark 4. One can notice that the optimisation in (10) assumes the availability of n_a-step ahead predictions of a measured disturbance d, however, this may not always be the case.

Corollary 1. Given a set of n_a-step ahead predictions of d_1 and the current estimate of d_2 ($d_{2k} = d_{2k+1} = ... = d_{2ss}$), then the optimization required will take the form:

$$\min_{\underset{\rightarrow}{\bar{u}}} \quad \underset{\rightarrow k-1}{\bar{u}}^T S \underset{\rightarrow k-1}{\bar{u}} + \underset{\rightarrow k-1}{\bar{u}}^T L \bar{z}_k + \underset{\rightarrow k-1}{\bar{u}}^T M \underset{\rightarrow k-1}{\bar{d}_1} \quad \text{s.t.} \quad \beta \underset{\rightarrow}{\bar{u}} \leq \gamma \tag{20}$$

Proof. This falls directly out of the optimisation in (10). The assumption $d_{2k} = d_{2k+1} = ... = d_{2ss}$ implies $\underset{\rightarrow k-1}{\bar{d}_2} = 0$. □

Local feedforward dual mode MPC 1-n_a-step ahead (LFFMPC1-n_a-step ahead)

1: Given an operating point and the local process model in (9), define the parameters in (20).
2: At each sampling instant, perform the optimization in (20).
3: Solve for the first element of $\underset{\rightarrow}{\bar{u}}$ and implement on process.

Note that the current estimate of d_2 at sample time k is handled implicitly by the optimisation in (20). Note also that the optimisation in (20) suggests that an assumption needs to be made regarding the estimation of the steady-state value d_{1ss} in order to ensure a systematic inclusion of integral action.

Remark 5. For a set of n_a-step ahead predictions of a measured disturbance d, the estimated steady-state value d_{ss} is assumed[2] to be equal to d at sample time $k + n_a$.

Remark 6. Note that a set of n_a-step ahead predictions of a measured disturbance d is considered by the optimisation in (20) if and only if $n_a \leq n_c$.

Corollary 2. Given the current estimates of d_1 and d_2 ($d_{1k} = d_{1k+1} = ... = d_{1ss}$ and $d_{2k} = d_{2k+1} = ... = d_{2ss}$), then the optimisation required will take the form:

$$\min_{\underset{\rightarrow}{\bar{u}}} \quad \underset{\rightarrow k-1}{\bar{u}}^T S \underset{\rightarrow k-1}{\bar{u}} + \underset{\rightarrow k-1}{\bar{u}}^T L \bar{z}_k \quad \text{s.t.} \quad \beta \underset{\rightarrow}{\bar{u}} \leq \gamma \tag{21}$$

It is clear from the optimisation in (21) that $\underset{\rightarrow k-1}{\bar{d}_1} = \underset{\rightarrow k-1}{\bar{d}_2} = 0$ which implies that the current estimates of d_1 and d_2 at sample time k are dealt with implicitly.

[2]This is validated in the next section through simulation.

Local feedforward dual mode MPC 1 (LFFMPC1)

1: Given an operating point and the local process model in (9), define the parameters in (21).
2: At each sampling instant, perform the optimization in (21).
3: Solve for the first element of $\underset{\rightarrow}{\bar{u}}$ and implement on process.

Similar to the LMPC, the LFFMPC1 can also be easily modified to cover a wide range of operation through gain scheduling.

GS feedforward dual mode MPC (GSFFMPC)

1: For each of the nominal operating points and given the local process model in (9), define the parameters in (21).
2: For a selected local controller and at each sampling instant, perform the optimization in (21).
3: Solve for the first element of $\underset{\rightarrow}{\bar{u}}$ and implement on process.

4.3. Alternative Formulations of LFFMPC1

Alternative formulations of LFFMPC1 can be obtained by making different assumptions about the models of the measured disturbances and the number of measured disturbances available.

So far, it has been assumed that the models of the measured disturbances are obtained through system identification as discussed in the previous section, however, as it has been pointed out in Section 2, the measured disturbances can also be modelled from first principles and hence an equivalent algorithm to LFFMPC1 can be developed as follows.

Local feedforward dual mode MPC 2 (LFFMPC2)

1: For a given operating point, represent the dynamic model in (4) in a discrete-time state space form using a sampling time of 39 s (process sampling time).
2: Given the local process model in (9), define the parameters in (21).
3: At each sampling instant, perform the optimization in (21).
4: Solve for the first element of $\underset{\rightarrow}{\bar{u}}$ and implement on process.

Another alternative of LFFMPC1 can be obtained by making an assumption that only a single measured disturbance is available.

Local feedforward dual mode MPC 3 (LFFMPC3)

1: Given an operating point and the local process model in (9) and assuming a single measured disturbance ($\bar{x}_k^{d_2} = \bar{d}_{2k} = 0$), define the parameters in (21).
2: At each sampling instant, perform the optimization in (21).
3: Solve for the first element of $\underset{\rightarrow}{\bar{u}}$ and implement on process.

4.4. Summary

This section has discussed a number of variants of dual mode MPC tailored to the application at hand. While the main contribution is the proposed GSFFMPC, the other proposed algorithms are equally important to highlight issues like the significance of sufficient modelling of the measured disturbances of the plant and the impact of considering the future behaviour of a measured disturbance along a given prediction horizon as will be shown in the next section.

For a better insight into the different dual mode MPC algorithms and before moving to the next section, Table 4 lists all the discussed algorithms and shows their distinct features.

Table 4 Dual mode MPC algorithms

Algorithm	Feedforward	Gain scheduling	Comments
LMPC	No feedforward action	No gain scheduling	Proposed in [15] and the model used is obtained through system identification
GSMPC	No feedforward action	Includes gain scheduling	Proposed in [11] and the models used are obtained through system identification
LFFMPC1-n_a-step ahead	Takes into account n_a-step ahead of d_1 and the current measurement of d_2	No gain scheduling	Models of the measured disturbances are obtained through system identification
LFFMPC1	Takes into account the current measurement of d_1 and d_2	No gain scheduling	Models of the measured disturbances are obtained through system identification
GSFFMPC	Takes into account the current measurement of d_1 and d_2	Includes gain scheduling	Models of the measured disturbances are obtained through system identification
LFFMPC2	Takes into account the current measurement of d_1 and d_2	No gain scheduling	Model of the measured disturbances is derived from first principles and based on steady-state conditions
LFFMPC3	Takes into account the current measurement of d_1 and not of d_2	No gain scheduling	Model of the single measured disturbance is obtained through system identification

5. Simulation Results

The impact of the different assumptions made in the previous section about the future of the measured disturbances is explored here. More specifically, this section aims to:

- Show the efficacy of the proposed GSFFMPC during the transient phase, set point tracking and disturbance rejection.
- Emphasise the significance of sufficient modelling of the measured disturbances of the plant.
- Draw attention to the impact of considering the future behaviour of solar radiation along a given prediction horizon.

Three different scenarios have been designed in order to meet these aims, but before proceeding any further with these scenarios, some preliminaries are discussed first.

5.1. Preliminaries

The plant is represented by the nonlinear simulation model described by the system in (2) with a slight increase to thermal losses in order to make the scenarios more realistic. Field inlet temperature ($T_{f,inlet}$) and ambient temperature (T_a) are kept fixed at $189°\mathrm{C}$ and $28°\mathrm{C}$ respectively. Even though this may not be the case in the normal operation of the plant, this is still a reasonable assumption during the steady-state phase. The HTF is assumed to be the synthetic oil Therminol® 55 and constrained to the range $0.002-0.012 m^3/s$, where the minimum limit is normally for a safety reason. Exceeding a temperature of $305°\mathrm{C}$ puts the synthetic oil at the risk of being decomposed. The difference between the field inlet-outlet temperature is also constrained not to exceed $80°\mathrm{C}$ in order to avoid the risk of oil leakage [1]. The latter has been taken care of implicitly when the nominal operating points and the desired reference temperature were selected. The HTF flow rate constraints are considered explicitly in the control design process as will be demonstrated in the following scenarios.

5.2. Gain Scheduled Feedforward Control

The following scenario shows the efficacy of the proposed GSFFMPC compared to the previously proposed GSMPC [11], that is, it demonstrates the benefits of utilising feedforward information where available. The scenario is shown in Fig. 5, it starts with a clear day and slowly time-varying solar radiation. During the transient phase ($9 - 9.15\ h$) and while the GSFFMPC is performing very well with fast transients and no overshoot, the GSMPC has somewhat poorer performance with a large overshoot around $13\ °\mathrm{C}$ and an oscillatory control signal.

As the day goes by a sudden drop in solar radiation occurs at $13.15\ h$ due to a passing and persistent cloud. As can be clearly seen in Fig. 5, the GSFFMPC performs better than the GSMPC with much less deviation from the desired reference temperature and a faster recovery time. Here again, the control signal of the GSMPC is slightly oscillatory. Set point tracking performance has been also evaluated for both algorithms over a short period of time during steady-state; Table 5 shows a numerical set point tracking performance of both algorithms over a period of $42\ m$ ($11.16-11.58\ h$). The GSFFMPC achieves lower root mean square error (RMSE) with a reduction of approximately $12.55\ \%$.

Table 5 Set point tracking performance

Algorithm	RMSE ($^{\circ}\mathrm{C}$)
GSMPC	0.0271
GSFFMPC	0.0237

5.3. Local Feedforward Control

The scenario in Fig. 6 demonstrates locally the importance of sufficient modelling of the field inlet temperature and solar radiation, even when the system uses a single controller, that is no gain scheduling. In particular, it highlights the superiority of the LFFMPC1 over the LMPC, LFFMPC2 and LFFMPC3.

Controllers are designed around the nominal operating point 0.006 m^3/s and similar to the scenario in Fig. 5, the scenario in Fig. 6 starts with a clear day and slowly time-varying solar radiation. During the transient phase ($9 - 9.26\ h$), LMPC (which has no feedforward action) has the worst control performance with significant overshoot around $17\ ^{\circ}\mathrm{C}$ and a substantial oscillatory control signal. The LFFMPC2 has better performance than LMPC with a noticeable improvement in the overshoot (being around $9.5\ ^{\circ}\mathrm{C}$) and slight improvement in the control signal. Best control performance is indeed exhibited by the LFFMPC1 with no overshoot and relatively smooth control signal.

Note that the LFFMPC3 is designed based on the dynamics of the volumetric flow rate of the HTF and solar radiation. In other words, dynamics of the field inlet temperature are not considered in the control design process. The impact of not considering the dynamics of the field inlet temperature on the transient phase is fairly obvious. One would expect a large overshoot and quite oscillatory control signal.

Fig. 6 also shows the behaviour of the four controllers during a sudden drop in solar radiation across the period $12.45 - 13.15\ h$. While the impact of the passing cloud on the LFFMPC1 is barely noticed, the LMPC gives notably poorer performance. The LFFMPC2 has a less effective use of the feedforward information and gives a seriously poor control signal whereas, as expected, the LFFMPC3 shows a similar response to LFFMPC1.

Table 6 gives numerical comparison of set point tracking performance during steady-state ($10.37 - 11.42\ h$). Clearly, the LFFMPC1 and LFFMPC3 give the lowest RMSE. Note that the set point tracking performance of the LFFMPC2 is still better than the LMPC.

Table 6 Local set point tracking performance

Algorithm	RMSE ($^{\circ}\mathrm{C}$)
LMPC	0.0413
LFFMPC1	0.0130
LFFMPC2	0.0207
LFFMPC3	0.0130

In summary, the LFFMPC1 has demonstrated that incorporating sufficient dynamic models of solar radiation and the field inlet temperature can significantly improve the control performance during the transient phase, set point tracking and disturbance rejection.

5.4. Measured Disturbances Along a Given Prediction Horizon

This part of the section investigates the impact of incorporating the expected future behaviour of solar radiation for a given prediction horizon. The performance of the LFFMPC1 for the current incident solar radiation is compared to the performance of the LFFMPC1 when the solar radiation is predicted 50-step ahead (32.5 min). The scenario here is quite extreme. Fig. 7 shows drastic changes in solar radiation due to thick and scattered passing clouds.

Just before $12.15\ h$, the performance of the LFFMPC1 is fairly similar to the performance of the LFFMPC1-50-step ahead. After $12.15\ h$ and due to the strong disturbances, some differences started to emerge, yet, the impact of the prediction capabilities is not quite clear. Hence Table 7 shows an online performance measure (J) of both algorithms.

Table 7 Online performance measure (J)

Algorithm	J
LFFMPC1	7570.1
LFFMPC1-50-step ahead	7398.6

The LFFMPC1-50-step ahead gives the lowest numerical value to the cost. Note that, however, the choice of 50-step ahead here is not optimal and needs further investigation.

As a final remark here, the steady-state value of a measured disturbance d was defined earlier as d at sample time $k + n_a$ and in order to validate this assumption, a typical daily cycle of solar radiation on a clear day is simulated. The cycle has a mean value of 800 W/m^2 and covers a range of 5 h 27 min and 36 s (504 samples). Fig. 8 shows the deviation of solar radiation after applying the LFFMPC1-50-step ahead for a desired reference temperature of 237 $^{\circ}$C. The deviation can be clearly seen converging to zero for each sample time k.

6. Conclusion

This paper has discussed the main feedforward approaches that have been proposed over the years for the ACUREX distributed solar collector field as well as the need for the development of a new feedforward approaches. Moreover, the paper has shown that the dynamics of the field outlet temperature due to changes in solar radiation are very similar to the dynamics of the field outlet temperature due to changes in the volumetric flow rate of the HTF, which is consistent with the experimental findings in [10] and the analysis in [3].

This paper has also taken the analysis of the measured disturbances of the ACUREX plant a step further by investigating the dynamics of the field inlet temperature and showing that indeed fast and abrupt changes in the field inlet temperature can excite the resonance dynamics of the plant.

The GS predictive control strategy proposed in [11] is improved in this paper by including the effects of the measured disturbances of the ACUREX plant in the predictions of future outputs (systematic feedforward design). Using a validated nonlinear simulation model of the ACUREX plant, models of the measured disturbances are estimated around a family of operating points directly from input-output data using the subspace identification method N4SID while taking into account the frequency response of the plant.

Simulation results have shown that incorporating sufficient dynamic models of the measured disturbances can significantly improve the control performance during the transient phase, set point

tracking and disturbance rejection. The results have also shown that deriving a dynamic model of the measured disturbances from first principles and based on steady-state conditions is an underestimation of their actual dynamics, which thus can result in a poor control performance during disturbance rejection.

Finally, the paper has attempted to draw attention to the impact of considering the future behaviour of solar radiation along a given prediction horizon. Even though the results were positive, one might argue that the improvements over that current incident solar radiation are not that significant. It is worth noting that questions like "How far ahead should one predict?" and accordingly "How significant the improvements can be?" still need to be answered.

Acknowledgements

The authors would like to thank Robin De Keyser and Clara Ionescu from Ghent University, Belgium for their cooperation and providing us with measured data to validate the proposed nonlinear simulation model. The first author would like also to thank the University of Jordan, Jordan for sponsoring his PhD studies.

7. References

[1] E. F. Camacho, M. Berenguel, F. R. Rubio, and D. Martínez, *Control of solar energy systems*. Springer-Verlag, 2012.

[2] E. Camacho, F. Rubio, and F. Hughes, "Self-tuning control of a solar power plant with a distributed collector field," *IEEE control Systems*, vol. 12, no. 2, pp. 72–78, 1992.

[3] A. Meaburn and F. Hughes, "Feedforward control of solar thermal power plants," *Journal of solar energy engineering*, vol. 119, no. 1, pp. 52–60, 1997.

[4] R. Silva, L. Rato, J. Lemos, and F. Coito, "Cascade control of a distributed collector solar field," *Journal of Process Control*, vol. 7, no. 2, pp. 111–117, 1997.

[5] A. Cardoso, J. Henriques, and A. Dourado, "Fuzzy supervisor and feedforward control of a solar power plant using accessible disturbances," in *European Control Conference, 1999*, pp. 1711–1716, IEEE, 1999.

[6] T. A. Johansen and C. Storaa, "Energy-based control of a distributed solar collector field," *Automatica*, vol. 38, no. 7, pp. 1191–1199, 2002.

[7] C. M. Cirre, M. Berenguel, L. Valenzuela, and R. Klempous, "Reference governor optimization and control of a distributed solar collector field," *European Journal of Operational Research*, vol. 193, no. 3, pp. 709–717, 2009.

[8] J. Álvarez, L. Yebra, and M. Berenguel, "Adaptive repetitive control for resonance cancellation of a distributed solar collector field," *International Journal of Adaptive Control and Signal Processing*, vol. 23, no. 4, pp. 331–352, 2009.

[9] M. Beschi, S. Dormido, J. Sanchez, A. Visioli, and L. J. Yebra, "Event-based pi plus feedforward control strategies for a distributed solar collector field," *IEEE Transactions on Control Systems Technology*, vol. 22, no. 4, pp. 1615–1622, 2014.

[10] A. Meaburn and F. Hughes, "Resonance characteristics of distributed solar collector fields," *Solar Energy*, vol. 51, no. 3, pp. 215–221, 1993.

[11] A. Alsharkawi and J. Rossiter, "Gain scheduling dual mode mpc for a solar thermal power plant," in *10th IFAC Symposium on Nonlinear Control Systems*, 2016.

[12] A. Alsharkawi and J. Rossiter, "Dual mode mpc for a concentrated solar thermal power plant," *IFAC-PapersOnLine*, vol. 49, no. 7, pp. 260–265, 2016.

[13] M. Gálvez-Carrillo, R. De Keyser, and C. Ionescu, "Nonlinear predictive control with dead-time compensator: Application to a solar power plant," *Solar energy*, vol. 83, no. 5, pp. 743–752, 2009.

[14] P. Van Overschee and B. De Moor, *Subspace identification for linear systems: Theory-Implementation-Applications*. Springer Science & Business Media, 1996.

[15] J. A. Rossiter, *Model-based predictive control: a practical approach*. CRC press, 2003.

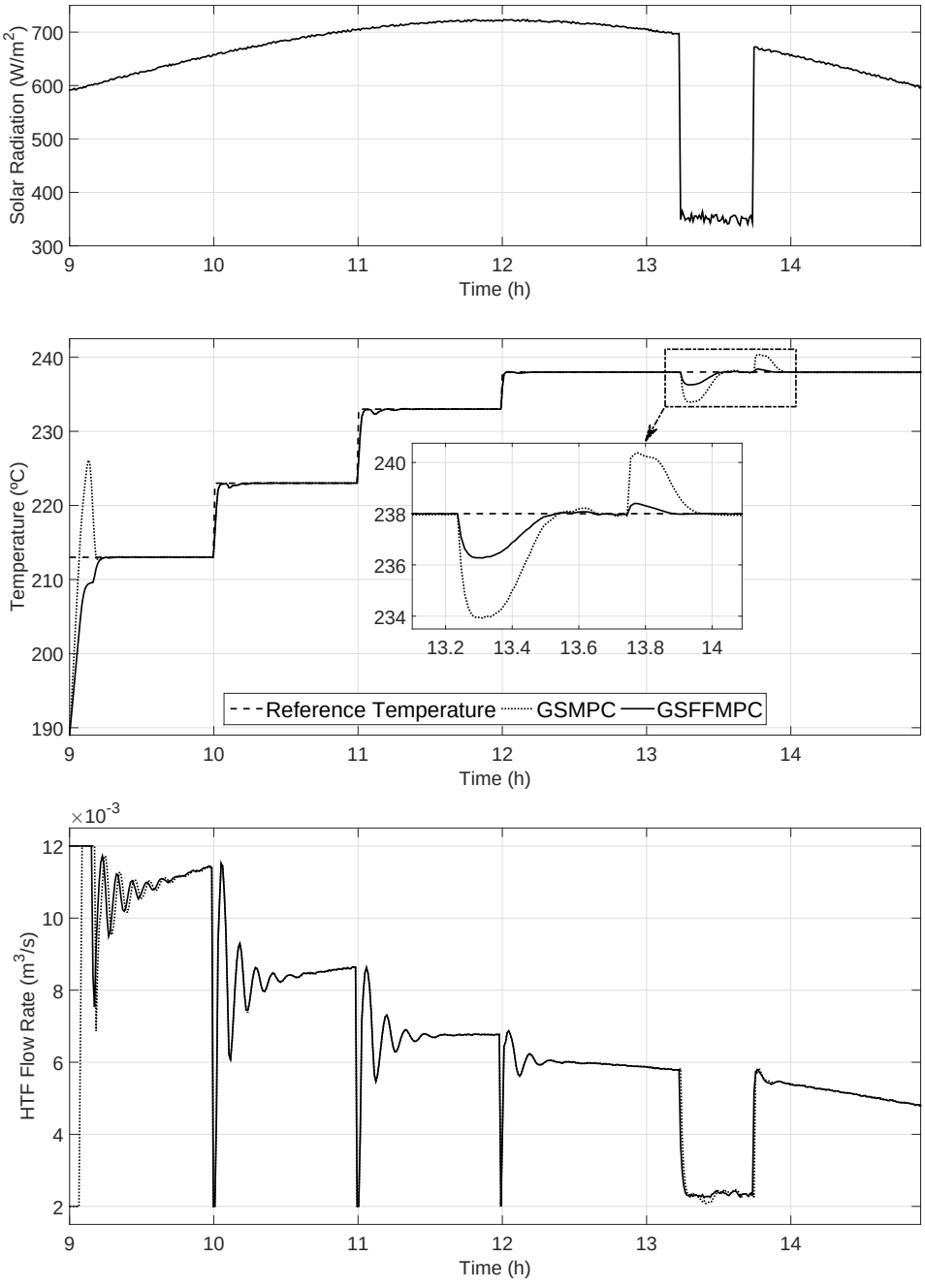

Fig. 5: A performance comparison: GSMPC against GSFFMPC.

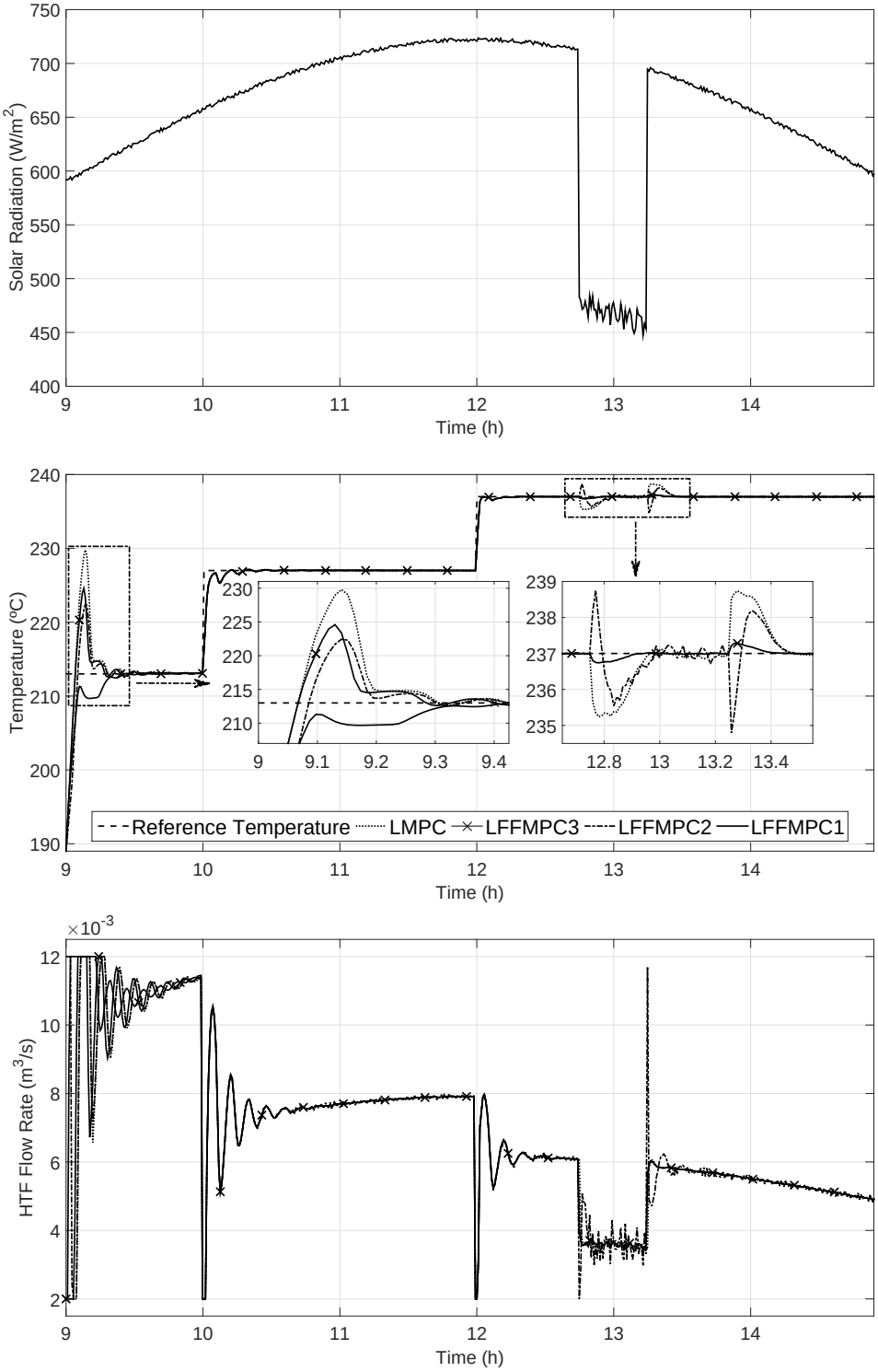

Fig. 6: A local performance comparison.

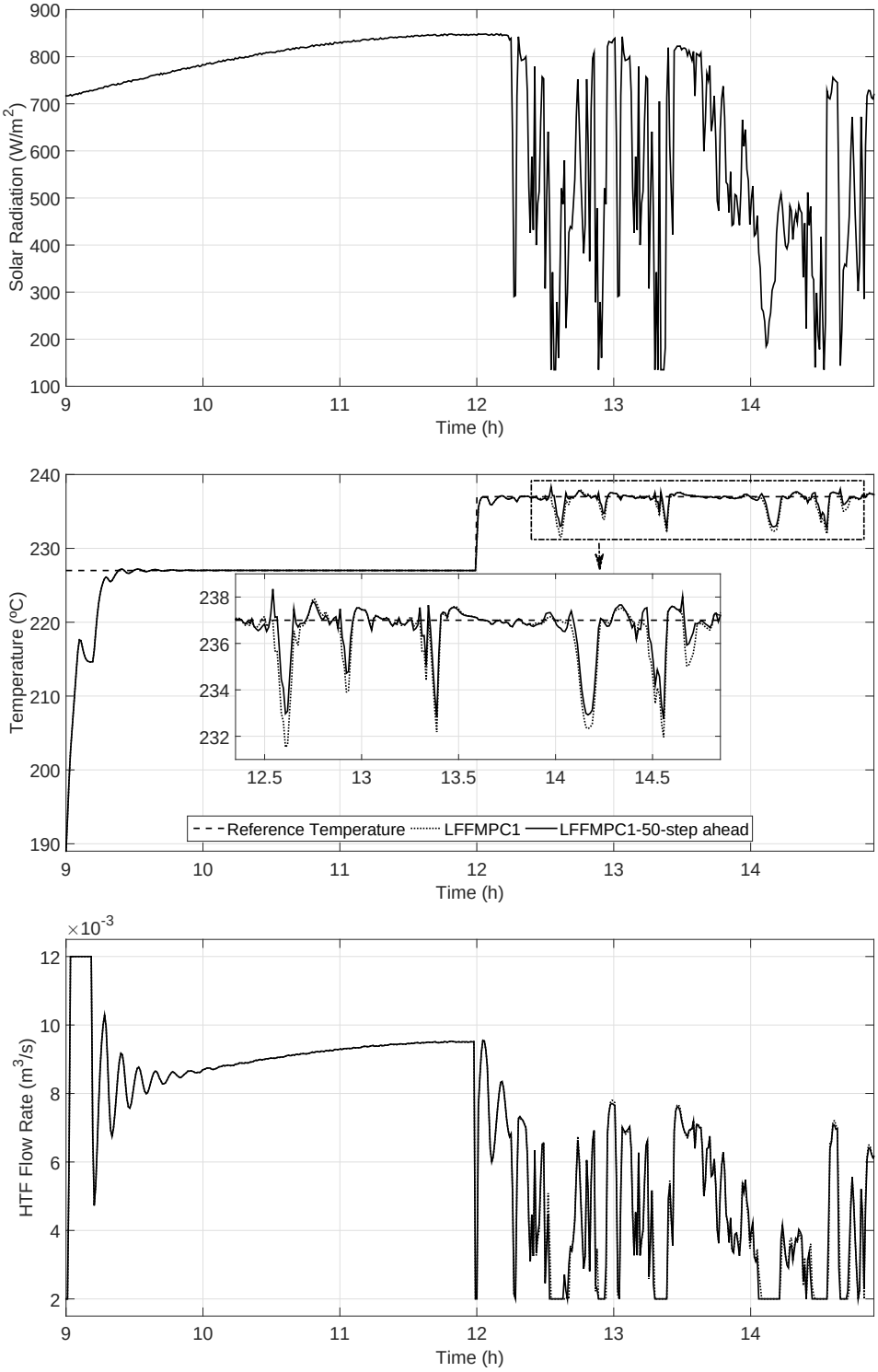

Fig. 7: A local performance comparison: LFFMPC1 against LFFMPC1-50-step ahead.

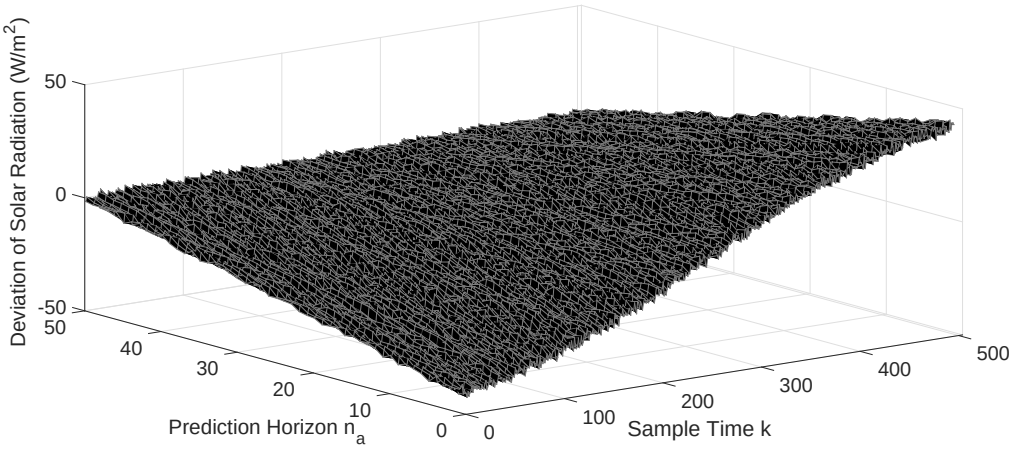

Fig. 8: Deviation of solar radiation from an estimated steady-state value.